Nanotechnology for Environmental Engineering (2026) 11:105
https://doi.org/10.1007/s41204-026-00594-1

ORIGINAL PAPER

Green-engineered Ag-Ni-Co trimetallic nanocomposite: a unified platform for visible-light photocatalysis and bioactivity

Pavan Sai Nagilla[1,2] · Sai Prudhvi Karanam[1,2] · Nithin Krishna Nagella[1,2] · Yasaswi Khaderbad[3] · Naveen Kumar Dabbeta[1,4] · Pranay Bhasker Kalakonda[5] · Balaji Pandya[4] · Vijay Morampudi[3] · Krishnakumar Balu[6] · Parvathalu Kalakonda[1,7]

Received: 20 June 2026 / Accepted: 26 July 2026

Abstract

Multifunctional nanomaterials often sacrifice depth per function, but the goal is not to outperform a single-function material. Here, we address this by reporting a *Camellia sinensis*-mediated Ag-Ni-Co trimetallic nanocomposite (TMNC) designed primarily for visible-light photocatalysis, with secondary evaluation of bioactivity. Unlike physical mixtures of mono- or bimetallic nanoparticles, this TMNC forms a crystalline heterojunction (crystallite size 12–25 nm, direct band-gap 3.1 ± 0.05 eV) with a Co-rich composition (50.2 wt% Co, 45.2% Ni, 4.6% Ag). At an optimized loading of 20 mg, the TMNCs achieves ≥ 98% degradation (decolorization) of methylene blue (MB) in 60 min, as monitored by UV-Vis spectroscopy ($k = 0.0472\ min^{-1}$), outperforming its monometallic and bimetallic counterparts. Mechanistically, the TMNCs architecture suppresses charge recombination, sustaining superoxide and hydroxyl radical flux. The same material also exhibits dose-dependent antibacterial activity against Enteropathogenic Escherichia coli **(EPEC)** (11.2 mm zone) and selective cytotoxicity against human colon cancer HCT-116 cells, linked to mitochondrial reactive oxygen species (ROS) generation. By anchoring the claim in quantitative photocatalytic kinetics and bioactivity as supporting evidence, this work establishes a reproducible, green-synthesized TMNCs platform for integrated environmental and biomedical applications.

Keywords Trimetallic nanocomposites · Green synthesis · Antibacterial · Anticancer · Catalytic activity

✉ Parvathalu Kalakonda
parvathalu@wpi.edu

Pavan Sai Nagilla
pavansai5031@mail.com

Sai Prudhvi Karanam
prudvik180@mail.com

Nithin Krishna Nagella
aellanitin@mail.com

Yasaswi Khaderbad
yasaswi.khaderbad@uohyd.ernet.in

Naveen Kumar Dabbeta
25enp01@uoyd.ac.in

Pranay Bhasker Kalakonda
pbkalako@ncsu.edu

Balaji Pandya
balajipadya@uohyd.ac.in

Vijay Morampudi
vijaymorampudi@uohyd.ac.in

Krishnakumar Balu
chemkrishna2006@yahoo.co.in

[1] Department of Physics, Smart Nanomaterial Research Laboratory, Government City College (A), Osmania University, Hyderabad TG 500002, India

[2] Department of Physics, Osmania University, Hyderabad TG 500007, India

[3] Department of Biochemistry, University of Hyderabad, Hyderabad TG 500046, USA

[4] School of Engineering Science and Technology (SEST), University of Hyderabad, Hyderabad TG 500046, India

[5] Department of Materials Science and Engineering, North Carolina State University, Raleigh NC 27695, USA

[6] Department of Chemistry, Karpagam Academy of Higher Education (Deemed to be University), Coimbatore -641 021, Tamilnadu, India

[7] Saveetha School of Engineering, Saveetha Institute of Medical and Technical Sciences (SIMATS), Chennai 602105, Tamilnadu, India

Published online: 12 August 2026

Abbreviations

TMNCS	Trimetallic Nanocomposites
UV-Vis	Ultra-violet visible spectroscopy
XRD	X ray diffraction
FTIR	Fourier transform infrared spectroscopy
SEM	Scanning electron Microscopy
MIC	minimum inhibition concentration
EPEC	Enteropathogenic Escherichia coli
MB	Methylene blue
ROS	Reactive oxygen species

Introduction

The global challenge of antibacterial resistance, together with the need for precise cancer treatments and sustainable environmental remediation, demands innovative multifunctional nanocomposite materials. Bio-nanotechnology represents a dynamic and integrative frontier, combining fundamental scientific principles with advanced engineering to develop multi-metallic nanoparticle systems. These composite architectures possess distinctive multifunctional capabilities, making them effective across biomedical innovation and environmental remediation applications [1–4]. Synthesized through a diverse array of fabrication techniques, metal nanoparticles demonstrate exceptional functional adaptability, enabling their deployment in critical biomedical roles such as anticancer and antimicrobial therapeutics [5, 6], as well as across pivotal sectors including energy storage systems, agricultural enhancements, sensor technologies, water purification methodologies, and the development of advanced materials for intelligent electronics [7–10].

The limitations of conventional antibiotics and anticancer therapies [1, 2], compounded by the global crisis of antimicrobial resistance, have created an urgent need for innovative therapeutic agents [3]. In response, significant research is focused on developing novel, multifunctional metal nanomaterials synthesized through sustainable, eco-friendly methods [4]. Green synthesis, which utilizes biological extracts to fabricate metal nanoparticles, presents a promising alternative multifunctional solution [3, 5, 6]. Green synthesis approach can produce dual functionality capable of simultaneously addressing multiple challenges: combating resistant infections, providing selective anticancer activity, and removing contaminants & toxic molecules from water bodies. Consequently, metal nanocomposite materials such as green-synthesized mono-metallic (MMNPs) [7–11], bimetallic (BMNPs) [12–18], and trimetallic nanoparticles (TMNPs) [19] have emerged as highly promising candidates for advanced biomedical applications and environmental remediation, representing a convergent solution to critical global health and industrial challenges.

The strategic integration of silver (Ag), nickel (Ni), and cobalt (Co) precursors in this nanocomposite is designed to exploit physicochemical properties that are difficult to achieve with mono- or bimetallic counterparts. Ag provides antimicrobial and plasmonic functionality, while Ni introduces catalytic sites and facilitates interfacial electron transfer. The inclusion of cobalt, particularly in oxide form, imparts magnetic recoverability and redox versatility, enhancing both practicality and oxidative potential. Together, these nanoscale components form an interactive synergistic composite system in which the combined material performance exceeds the contribution of each individual metal. Consequently, this work introduces green-synthesized Ag-Ni-Co TMNCs as an integrated reactive system designed to address three challenges: eradicating resistant pathogens, selectively targeting cancer cells, and catalytically degrading organic aquatic pollutants.

The synthesis of metal nanoparticles relies on diverse methodologies, ranging from conventional chemical reduction and microwave-assisted techniques to environmentally benign biosynthetic routes using plant extracts [20, 21]. While established, chemical methods frequently entail complex protocols, high costs, and the generation of toxic residues, raising significant environmental and biosafety concern [22–27]. In contrast, the pursuit of sustainable alternatives has driven research into multi-metallic systems. Earlier investigations established mono- and BMNPs as promising antibacterial agents, leveraging core-shell architectures and ionic synergy [28–31]. Building on this, contemporary research is increasingly focused on advanced BMNPs and TMNCs [32–34]. These composite materials are being rigorously evaluated not only for enhanced antimicrobial efficacy & cytotoxicity, but also for their pivotal role in sustainable water purification technologies, addressing the critical need for wastewater remediation [35–38].

In this work, we present a green route for preparing an Ag-Ni-Co TMNC using *Camellia sinensis* leaf extract as the reducing and stabilizing medium. The study focuses on how the combined presence of Ag, Ni, and Co influences the structural, catalytic, antibacterial, and anticancer properties of the material. Although mono- and bimetallic nanoparticles have been extensively investigated, reports on green-synthesized Ag-Ni-Co TMNCs systems remain not studied. Here, a single Ag-Ni-Co nanocatalyst system with an Ag: Ni: Co ratio of 1:9:10 is examined across three functional areas (novelty). The Co-rich TMNC shows efficient visible-light-assisted degradation of methylene blue, reaching ≥ 98% dye removal, along with measurable antibacterial activity and cytotoxic effects against cancer cells. These outcomes suggest that the interaction among the three

metals improves charge separation and supports reactive oxygen species generation (ROS), which may contribute to both photocatalytic and biological responses. Overall, the characterization and performance results indicate that this green-synthesized Ag-Ni-Co TMNCs can serve as a useful multifunctional platform for environmental remediation and biomedical research.

Methods and characterizations

Materials

$Co(NO_3)_2 \cdot 6\ H_2O$, $Ni(NO_3)_2 \cdot 6\ H_2O$, $AgNO_3$, and all other solvents were purchased from Sigma-Aldrich Pvt. Ltd., Bangalore, India. Fresh *Camellia sinensis* leaves were collected from Ooty, Nilgiris, Tamil Nadu, India.

Synthesis of nanoparticles

Green synthesis of TMNCs was performed using an aqueous plant leaf extract. For this process, 1 g of fresh *Camellia sinensis* (CS) leaves was steeped in 50 mL of deionized water to prepare the primary green extract, which was subsequently filtered to obtain a clear solution. This phytochemical-rich extract served as both the reducing and stabilizing agent. Separate aqueous solutions (50 mL each) of $Co(NO_3)_2 \cdot 6\ H_2O$, $Ni(NO_3)_2 \cdot 6\ H_2O$, and $AgNO_3$ were prepared in the stoichiometric ratio Ag: Ni: Co = 1:9:10. The individual precursor solutions were combined in a 200 mL beaker under magnetic stirring at 500 rpm and 80 °C to obtain a uniform mixture. The mixture was then ultrasonicated to ensure homogeneity and initiate nucleation for uniform TMNC formation.

Subsequently, the CS leaf extract was introduced dropwise using a standard laboratory burette into the combined precursor salt solution under vigorous stirring (600 rpm) at 85 °C. The reaction proceeded until a distinct color change and precipitate formation indicated successful synthesis of the Ag–Ni–Co TMNCs. The resulting TMNCs were isolated by filtration, thoroughly washed with deionized water and ethanol to remove residual impurities, and dried at 100 °C to obtain a fine powder. To verify the reliability and consistency of the synthesis process, the entire procedure was repeated multiple times. All experiments were performed in triplicate ($n = 3$) to confirm reproducibility. A schematic representation of the green synthesis process is provided in Fig. 1.

Characterization of synthesized nanoparticles

The formation of the Ag-Ni-Co TMNCs is confirmed by UV-visible spectroscopy. We employ FTIR spectroscopy to identify the surface biomolecules and phytochemicals responsible for nanoparticle nucleation and capping. FE-SEM reveals the material morphology, while coupled EDS confirms its elemental composition. XRD analysis determines the crystalline phase and estimates crystallite size. Finally, we calculate both direct and indirect optical band gaps from UV-Vis absorbance data using Tauc plot analysis. This suite of characterizations fully details the optical, morphological, and structural properties of the synthesized TMNCs.

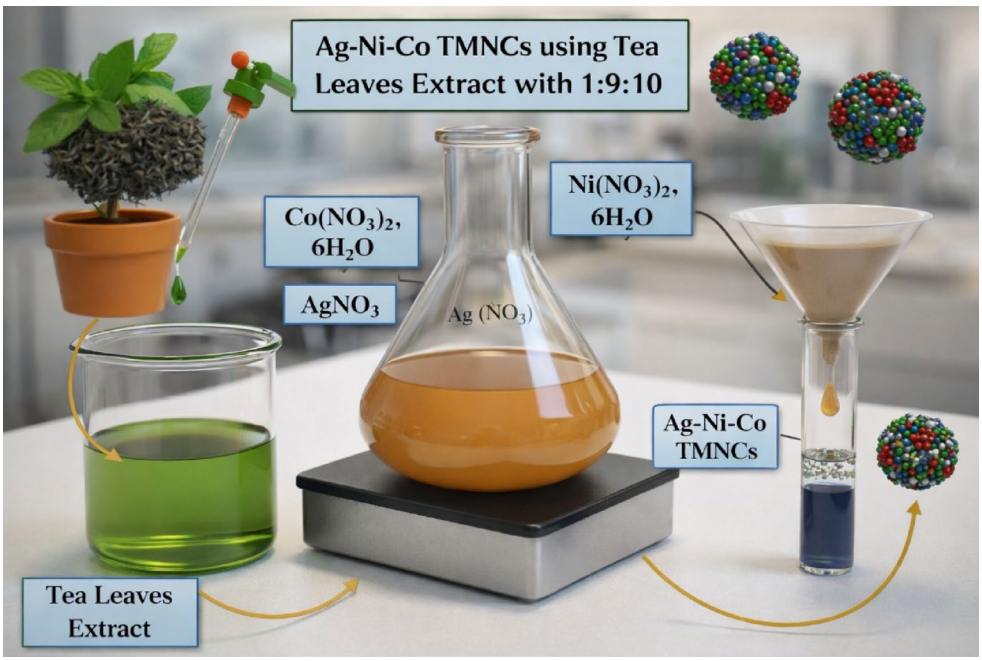

Fig. 1 Schematic of green synthesis process of CS leaf extract mediated Ag-Ni-Co TMNCs

Photocatalysis & dye degradation

We assessed the photocatalytic performance of the Ag-Ni-Co TMNC catalyst for MB dye degradation under visible light using a 20 W LED source. In a typical test, 20 mg or 30 mg of catalyst was dispersed in 5 mL of deionized water and added to a 10 ppm MB solution. The suspension was stirred in the dark for 15 min to reach adsorption–desorption equilibrium before light exposure. During irradiation, 3 mL aliquots were collected every 10 min for 60 min. Degradation progress was monitored by UV–Vis spectroscopy by measuring the decrease in MB absorbance at 668 nm. The percentage of dye degradation was calculated using the standard formula, based on the reduction in absorbance over time.

$$Degradation\ (\%) = (C_0 - C_t)/C_0$$

Where C_0 indicates the initial absorption, C_t indicates the absorption at a finite time t.

Antibacterial and anticancer activity

All antibacterial and cytotoxic evaluations are conducted under sterile conditions within a biosafety cabinet. The detailed procedure & protocol for the antibacterial assessment against EPEC follows the established methodology described in our prior work [39]. To ensure statistical robustness and reproducibility, both the antibacterial assays against **EPEC** and the anticancer assays utilizing **HCT116** cells are performed in independent triplicates.

Bacterial culture

The enteropathogenic EPEC strain, a gram-negative rod-shaped bacterium, is initially revived from glycerol stock cultures maintained at −80 °C. Revival was achieved by inoculating into LB broth, followed by overnight incubation at 37 °C with continuous agitation at 180 rpm [40]. This pre-culture is then used to inoculate fresh LB medium to facilitate active growth for subsequent experiments. For antibacterial testing, a standardized inoculum is prepared by adjusting the optical density of the overnight culture to an OD_{600} of 1. This standardized bacterial suspension is employed directly in both the agar well diffusion assay and for determining the direct inhibitory assay (DIA) [41].

Antibacterial activity: agar well diffusion and direct inhibition assays

The antibacterial efficacy of the Ag-Ni-Co TMNC against EPEC is evaluated using two standard assays. We first perform the agar well diffusion method. A standardized EPEC inoculum (1×10^9 CFU/mL, $OD_{600} = 1$) is uniformly swabbed onto L-S agar plates. Wells, 6 mm in diameter, are punched aseptically and loaded with 20 µL of the TMNC suspension at three concentrations: 1, 1.5, and 2 mg/mL. Control wells receive 20 µL of the precursor tea extract and 20 µL of gentamicin (30 µg). After overnight incubation at 37 °C, the antibacterial activity is quantified by measuring the diameter of the inhibition zone around each well according to the established protocol [40].

Quantitative assessment is performed via a microdilution broth assay in 96-well plates. Each well contained a final mixture of 70 µL LB broth, 10 µL of the standardized bacterial culture, and 20 µL of the respective TMNC concentration (1, 1.5, 2 mg/mL). Control wells included a negative control (sterile distilled water in place of the nanocomposite) and a positive control (gentamicin, 30 µg). The initial optical density (OD_{600}) is recorded immediately (t=0 h) using a microplate reader. After 24 h of incubation at 37 °C, the final OD_{600} was measured. The growth (%) inhibition is estimated using the following method:

$$\textbf{Growth inhibition}\ (\%) = [\frac{\mathbf{\Delta C - \Delta T}}{\mathbf{\Delta C}} \times 100]$$

where ΔC refers to corrected absorbance of the negative control ($OD_{24h} - OD_{oh}$) and ΔT indicates the corrected absorbance of the test well ($OD_{24h} - OD_{0h}$). To corroborate the spectrophotometric data with a direct measure of bacterial viability, 10 µL aliquots from selected wells (serially diluted 10^1–10^6), plated onto LB agar, and incubated (overnight at 37 °C). The resulting colony-forming units (CFU/mL) are calculated to estimate the bactericidal effect of the TMNCs at each concentration [41].

Anticancer assay: Alamar blue assay

The cytotoxic activity of the synthesized Ag-Ni-Co TMNCs was tested on HCT116 human colorectal carcinoma cells obtained from NCCS, Pune. Cells were maintained in McCoy's 5 A medium supplemented with 10% FBS and 1% antibiotic–antimycotic solution at 37 °C in a 5% CO_2 atmosphere. For the assay, cells were seeded in 96-well plates at 1×10^4 cells per well and incubated overnight. They were then exposed to TMNC concentrations of 1, 1.5, and 2 mg/mL for 24 h. After treatment, 10 µL of resazurin solution (50 µg/mL) was added to each well. Following a 3 h incubation, fluorescence was recorded at 570/590 nm (excitation/emission) using a microplate reader. Cell viability was expressed as a percentage relative to the untreated control [59].

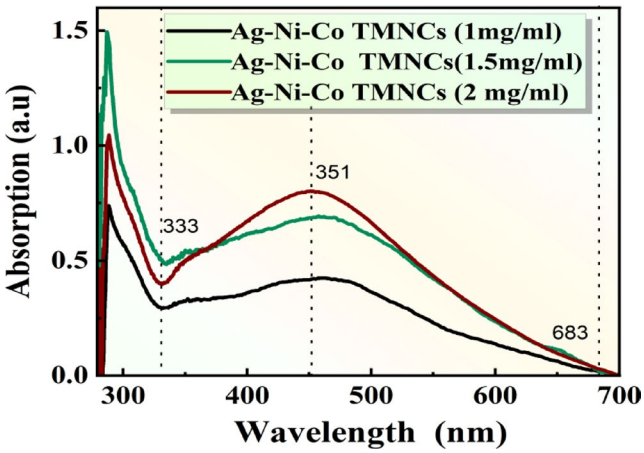

Fig. 2 UV-Vis absorption spectra of Ag-Ni-Co TMNC synthesized through CS leaf extract

$$\text{Cell viability } (\%) = \frac{\text{T}}{\text{R}} \times 100$$

where T is the Fluorescence value from the tested samples and R is the absorbance value from the control group. All reported data from well diffusion, direct inhibition, and anticancer activity assays represent the mean ± standard deviation (SD) of three technical replicates. Statistical significance is determined using one-way ANOVA ($p < 0.0249$). Graph Pad Prism software (v. 8.4) is employed for all graphing and statistical analysis.

Results and discussion

Synthesis and light absorption insights

UV-Vis absorption spectroscopy

The successful co-reduction of Ag^{+}, Ni^{2+}, and Co^{2+} ions mediated by CS leaf extract to form the TMNC is confirmed by UV-Vis spectroscopy (Fig. 2). The spectra of colloidal Ag-Ni-Co TMNC suspensions at varying concentrations (1–2 mg/mL) exhibit a distinct, concentration-dependent absorption profile. A prominent SPR band is observed at around 351 nm, which is characteristic of AgNPs but it is observed as blue shift by approximately 70 nm relative to the typical SPR of spherical AgNPs (~420 nm). This blue shift indicates strong electronic coupling between Ag, Ni, and Co within the TMNC structure, arising from changes in the local dielectric environment and intermetallic charge transfer. Furthermore, the spectra display a broad absorption tail extending from ~400 nm across the visible region, attributable to d–d transitions of Ni^{2+}/Ni^{3+} and Co^{2+}/Co^{3+} species. The absence of separate, sharp SPR features for individual metallic phases and the smooth, continuous

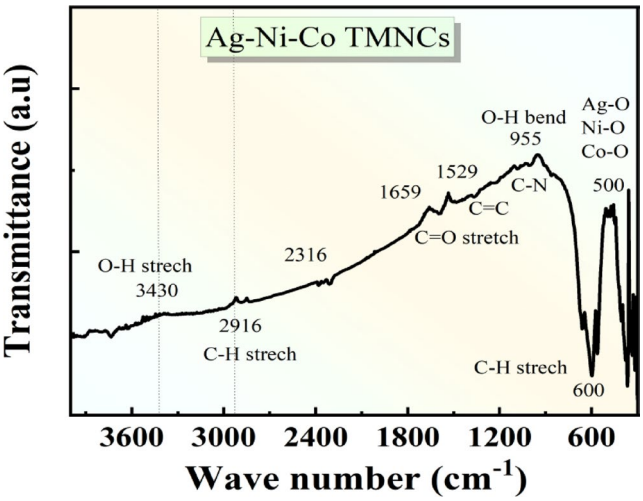

Fig. 3 FTIR spectrum of CS leaf extract mediated Ag-Ni-Co TMNCs

absorption profile support the formation of a homogeneous, electronically integrated TMNC rather than a physical mixture of monometallic particles. This intimate electronic interaction, facilitated by polyphenols and flavonoids in the CS leaf extract acting as reducing and capping agents, establishes the optical foundation for enhanced charge separation and ROS generation in the multifunctional catalytic and biocidal performance described in subsequent sections.

FTIR analysis

The FTIR profile of the CS leaf extract-mediated Ag-Ni-Co TMNCs confirms green synthesis and surface stabilization of the nanocomposite (Fig. 3). Key functional groups from the extract are evident on the TMNC surface. A broad O–H stretching vibration at 3430 cm^{-1} signifies hydroxyl groups from polyphenols, which facilitate metal-ion reduction and colloidal stability. A weak C–H stretching band at 2916 cm^{-1}, associated with phenolic compounds, suggests the presence of an organic capping layer. A prominent C = O stretching band at 1659 cm^{-1} indicates that carbonyl-containing compounds participate in metal coordination and surface passivation. Importantly, the spectrum shows characteristic metal–oxygen (Ag–O, Ni–O, Co–O) vibrations below 600 cm^{-1} and a C–N stretch near 955 cm^{-1}, confirming complexation of the three metals and their surface interactions with amine groups. Comparative FTIR analysis for both samples reveals significant spectral changes upon TMNC formation. The O-H stretching band shifts from 3400 cm^{-1} in the extract to 3430 cm^{-1} in the TMNC, accompanied by broadening, indicating coordination of phenolic -OH groups to metal ions. The C = O band shifts from 1640 to 1659 cm^{-1}, suggesting carbonyl-metal binding. The appearance of new M-O bands below 600 cm^{-1} confirms metal oxide formation. These spectral changes provide direct evidence for

the chemical interaction between phytochemicals and the TMNC surface, confirming the role of plant extract components as both reducing and capping agents.

Following the established green synthesis mechanism [42], the Camellia sinensis phytochemicals play sequential roles in TMNC formation. First, catechins reduce metal ions in the order of their standard reduction potentials ($Ag^{+} > Ni^{2+} > Co^{2+}$), creating Ag-rich core that facilitates nucleation. Second, the abundant polyphenols adsorb on the growing nuclei via coordination bonds, limiting particle growth and preventing extensive aggregation. Third, the quinone derivatives and intact catechins form a protective organic shell (confirmed by FTIR) that provides electrostatic and steric stabilization. This phytochemical control over nucleation, growth, and surface functionalization is critical for achieving the nanoscale dimensions and uniform composition of the TMNC. Collectively, the FTIR data verify that phytochemicals from CS leaf extract function as reducing, capping, and stabilizing agents during TMNC formation. [60, 61].

Morphology, composition and crystal structure

FE-SEM & EDS -morphology & elemental mapping

The surface details and elemental composition of green synthesized Ag-Ni-Co TMNCs are analyzed through FE-SEM and EDS (Fig. 4A, B & C). The FE-SEM micrographs reveal that quantitative analysis of 200 particles from multiple FE-SEM images reveals an average particle size of 190 ± 10.5 nm with a log-normal distribution (standard deviation 45 nm). Most nanoparticles (80%) fall within the 150–250 nm range. The significantly larger particle size compared to crystallite size (12–25 nm) indicates that each observed particle is an aggregate or cluster of smaller crystallites, consistent with the multi-phase nature of the TMNC. This aggregation increases the effective surface area while maintaining the nanoscale properties of the constituent crystallites.

The formation of these small, aggregated microstructures is interpreted as complex crystal growth kinetics and complexation process of these three different composite nano particles (Ag, Ni, and Co). The EDS composition analysis (Fig. 4D) confirms the presence of Ag, Ni, and Co as the main metal elements which also reveal weight percentages 50.2% for Co, 45.2% for Ni, and 4.6% for Ag. Elemental mapping (Fig. 4E-H) reveals the homogeneous distribution of Ag, Ni, and Co throughout the TMNC clusters. The uniform overlay suggests the formation of an integrated trimetallic structure rather than a physical mixture of individual particles. Slight enrichment of Co in the core regions, with Ni and Ag more evenly distributed, indicates controlled phase evolution during the green synthesis process. This homogeneity is critical for the synergistic interactions that underpin the multifunctional performance of the TMNC.

This specific Ag-Ni-Co stoichiometry is critical, as the incorporation of Ag into the Co-Ni matrix significantly alters the surface/plasmonic properties of the TMNC composite

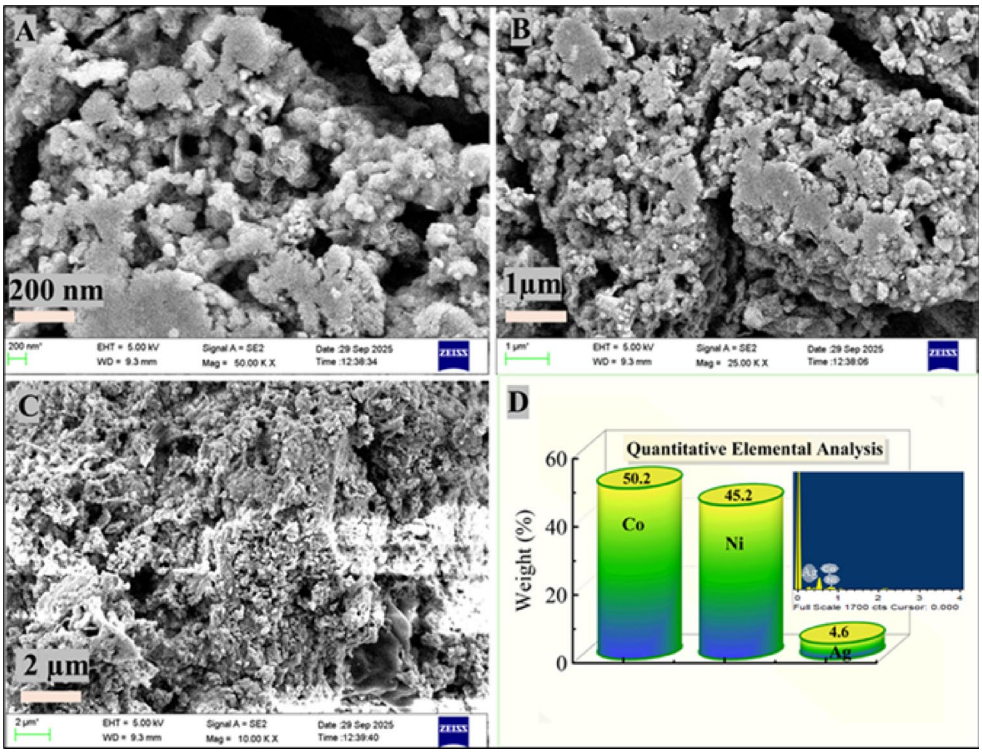

Fig. 4 (**A**, **B**, **C**) FE-SEM images of Ag-Ni-Co TMNCs showing uniform morphology; (**D**) EDS-quantitative composition

material. This tailored Ag-Ni-Co TMNCs configuration is directly relevant to its application, suggesting synergistic interactions among all three metals that enhance conductivity, provide active sites for catalysis, antibacterial, anticancer, and improve structural integrity under operational stresses, thereby establishing a direct correlation between the observed physicochemical characteristics and intended high-performance function. **This work is the first to report a green-synthesized Ag-Ni-Co trimetallic nanocrystal system with a composition notably enriched in cobalt and nickel relative to silver, facilitating the exploration of their synergistic potential.**

X-Ray diffraction (XRD)

The phase composition and crystallographic details of the green synthesized Ag-Ni-Co TMNCs are studied through XRD analysis. XRD profile reveals a multi-phase material system, with primary diffraction peaks corresponding to crystalline planes of the constituent metals (Ag, Ni, Co) and their oxides (Fig. 5A). The observed peaks at 29.5^0 (220), 43.3^0 (200), and 62.8^0 (220) are indexed to a Ni-rich phase ($Ag_{0.1}Ni_{0.9}$, PDF# 04–023-8782), while the peak at 45° (400) corresponds to cobalt oxide (Cobalt oxide, PDF# 04–005-9658). Characteristic silver reflections are present at 38.1^0 (111) and 77.4^0 (311), which match both metallic Ag and Ag_2O (PDF# 00–041-1104) phases. Additional minor phases identified include Co_3O_4 (01–071-4921), NiO_2 (04–010-4751), and a complex mixed-metal oxide phase ($AgCo_{0.5}Ni_{0.5}O_2$, PDF# 04–007-9667), indicating the formation of a composite with metallic and oxide components. The XRD Rietveld refinement (Fig. 5B) suggests the composite adopts **an O_3-type layered oxide structure with a rhombohedral R-3 m space group** [43], a specific stacking arrangement and symmetry class commonly found in alkali-metal intercalated transition metal oxides. The crystallite size, estimated from the Debye Scherrer model using the FWHM of the most intense peaks, falls within the range of 12 to 25 nm. The formation of a true trimetallic nanocomposite is supported by: (i) the presence of mixed-metal phases in XRD ($Ag_{0.1}Ni_{0.9}$, $AgCo_{0.5}Ni_{0.5}O_2$) that cannot arise from physical mixtures; (ii) the significant blue shift of the Ag SPR from 420 nm to 351 nm, indicating intermetallic electronic coupling; and (iii) the simultaneous presence of all three metals in individual clusters confirmed by EDS. The coexistence of metallic and oxide phases within a single nanostructure is characteristic of heterojunction formation, not physical aggregation. Uniquely, the TMNCs XRD profile displays overlap peaks and intensity modulations, reflecting synergistic interactions among multi-phase components (Cobalt oxide:28%; Ag-Ni-Co:24%; AgO:22%; Ni-Ag:15%; NiO:5%) that is distinct from the individual metal nanoparticles (**Fig. S1, see supporting information**). The incorporation of multiple metallic components induces significant lattice strain and defects within the TMNC structure. The estimated microstrain (0.2–0.4%) arises from the atomic radius mismatch between Ag (1.65 Å), Ni (1.24 Å), and Co (1.25 Å). This strain, combined with the coexistence of metallic and oxide phases, creates abundant interfacial defects and oxygen vacancies. According to recent studies [44, 45], such microstructural distortion can significantly influence photocatalytic behavior by modifying band edge positions, creating mid-gap states, and facilitating charge carrier separation. The observed superior photocatalytic performance of the TMNC can be partially attributed to these strain-induced effects. The nanoscale dimension,

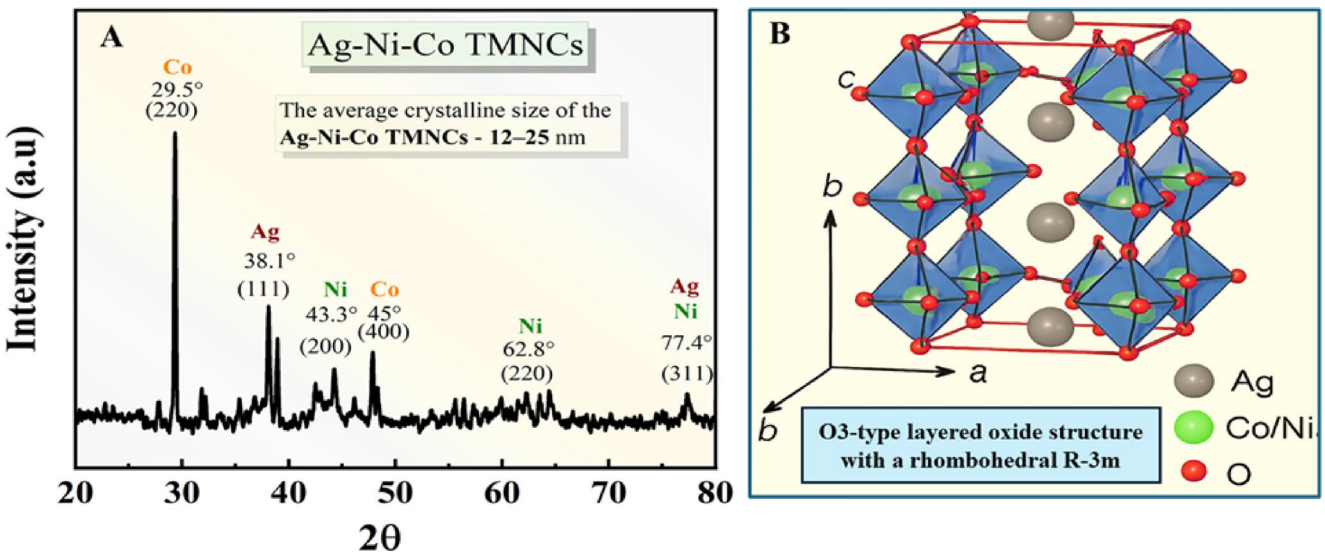

Fig. 5 **(A)** XRD pattern of green-synthesized Ag-Ni-Co TMNCs using *Camellia sinensis* (CS) leaf extract. (**B**) Proposed structural refinement model showing the O3-type layered oxide phase with rhombohedral R-3 m space group symmetry [43]

Table 1 Crystallite size calculation for Ag-Ni-Co TMNCs using the Debye-Scherrer equation

Phase	hkl Plane	2θ (deg)	FWHM (β) (rad)	Crystallite Size (nm)	Possible Structure
Ag/Ag_2O (00–041-1104) [46]	(111)	38.1	0.0060	22	FCC cubic
$Ag_{0.1}Ni_{0.9}$ (04–023-8782)	(220)	43.3	0.0055	24	Spinel
$Co_{0.5}Ni_{0.5}$ O(04–019-6384)	(400)	45	0.0072	24	FCC rock salt
$AgCo_{0.5}Ni_{0.5}O_2$ (04–007-9667) [47]	(400)	45	0.0065	20	Rhombohedral

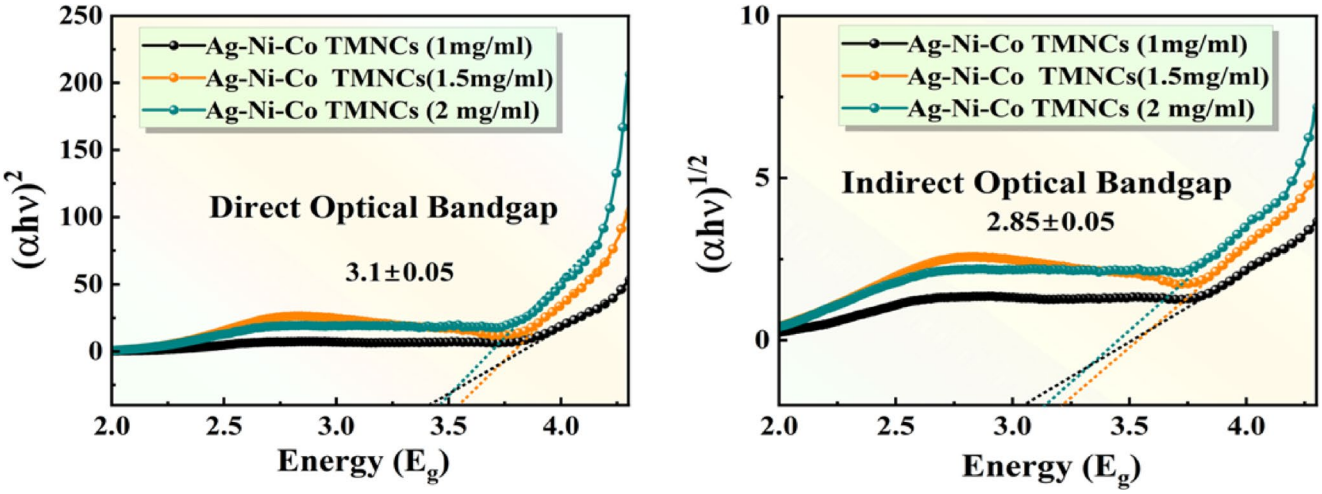

Fig. 6 Optical band gap for Ag-Ni-Co TMNCs via Tauc plot analysis (0.5, 1.0, and 1.5 mg/mL). (**A**) Tauc plot for direct band gap transition (**B**) Tauc plot for indirect band gap transition

combined with the identified coexistence of metallic and their oxide phases, is critical for the composite material's functional properties, as it suggests a high surface-to-volume ratio and the potential for synergistic surface interfacial effects between the phases, which are directly relevant to enhancing photocatalytic activity in advanced catalytic applications. The crystallite size of Ag-Ni-Co TMNCs are shown in Table 1.

Optical and electronic properties

The optical and electronic properties of the *CS plant leaves*-mediated Ag-Ni-Co TMNCs are studied through UV-Vis spectroscopy and Tauc plot analysis (Fig. 6A **&B**). As presented in the figure, the synthesized materials exhibit well-defined optical absorption characteristics. Using Tauc plot analysis with $(\alpha hv)^2$ for direct and $(\alpha hv)^{1/2}$ for indirect bandgaps, with proper baseline correction and zeroing of the y-axis, the direct bandgap is calculated as 3.15 ± 0.05 eV and the indirect bandgap as 2.85 ± 0.05 eV. The indirect bandgap in the visible range (~2.85 eV) is consistent with the observed visible-light photocatalytic activity. The presence of sub-bandgap states and Ag SPR further contributes to visible-light absorption. The values are in good agreement with the recommended literature [48] for multi-metal oxide systems.

While the direct bandgap of 3.4–3.5 eV suggests primarily UV absorption, the presence of an indirect bandgap (3.0–3.2 eV), broad visible absorption tail (400–800 nm), and Ag SPR effects collectively enable visible-light photocatalytic activity. The photogenerated charge carriers utilize sub-bandgap excitation pathways facilitated by the multi-metal synergy. This dual-bandgap nature suggests the material facilitates charge carrier generation through multiple pathways, which is a critical determinant of its functional efficacy. The relatively wide band gaps position these Ag-Ni-Co TMNCs as potential candidates for applications requiring UV-light absorption, such as photocatalysis for environmental remediation. Furthermore, the consistency of the band gap values across different sample densities confirms the homogeneity and reproducibility of the green synthesis process.

Catalytic performance: dye degradation, and mechanistic insights

Figure 7 **(a and b)** presents the UV-Vis absorption spectra for MB dye (10 ppm, pH 10) under visible light irradiation (20 W) in the presence of Ag-Ni-Co TMNC photocatalysts. The catalyst mass varies between 20 mg and 30 mg. The characteristic absorption maximum of MB, observed at approximately 668 nm, exhibits a pronounced and continuous rapid reduction in intensity as a function of irradiation

time (0 to 60 min). Control experiments confirmed that photocatalysis is the primary mechanism for MB degradation. In the absence of catalyst (photolysis), <5% degradation was observed over 60 min. Dark adsorption studies showed ~−10% adsorption of MB onto the TMNC surface, indicating that the observed>98% degradation in visible light is predominantly due to photocatalytic activity. This systematic attenuation of the primary absorption band provides direct spectroscopic evidence for the effective photodegradation of the MB dye molecules by the Ag-Ni-Co TMNC photocatalysts under the stated experimental conditions. The photodegradation for the two catalyst loadings (20 mg and 30 mg) both lead to nearly complete degradation (≥98%) of MB dye within 60 min (Fig. 8a **&** **b**). However, analysis of the temporal decay in absorbance at 668 nm reveals a more rapid initial degradation rate for the 20 mg loading, indicating a more efficient catalytic dye degradation performance at this lower loading catalyst loading. In contrast, the trajectory with 30 mg catalyst loading, though ultimately effective, suggests a marginally less uniform kinetic profile in the initial phases. This counter-intuitive finding where a lower catalyst loading delivers better overall performance highlights an optimized synergy between active site availability and reactive species generation, positioning the 20 mg loading of Ag-Ni-Co TMNCs as the more optimum efficacious configuration for rapid and thorough pollutant annihilation. UV-Vis spectroscopy confirms the disappearance of the MB chromophore at 668 nm, indicating effective degradation. However, complete dye degradation to CO_2 and H_2O would require additional TOC analysis, which will be addressed in future work. The experiments were repeated 3 times, and the results remained same. The complex mechanisms governing photo- dye degradation and provide a foundational framework for advancing catalyst design in environmental remediation.

Figure 8 presents a comparative kinetic analysis of the photocatalytic activity for Ag-Ni-Co TMNCs at 20 mg and 30 mg loadings under visible light irradiation. The degradation profiles (Fig. 8a and b) demonstrate that the 20 mg loading achieves a marginally higher percentage of MB dye degradation over the 60-minute period. This is further supported by the normalized concentration decay (C_t/C_0, Fig. 8c), which shows a more rapid decrease for the 20 mg catalyst, indicating superior initial photocatalytic dye degradation efficiency. Fitting the data to a pseudo-first-order kinetic model (Fig. 8d) yields rate constants (k) of 0.0472 min^{-1} for the 20 mg loading and 0.0364 min^{-1} for the 30 mg loading, with corresponding R^2 values of 0.98944 and 0.99863, respectively. Consequently, after 60 min, the system with 20 mg of catalyst attains near-complete degradation (~100%), exceeding the final efficiency of the 30 mg loading. These results collectively establish that the 20 mg loading exhibits the most effective photocatalytic performance, which is attributed to optimal charge carrier separation, reduced recombination, and enhanced light-harvesting capability, highlighting its potential for application in wastewater treatment. The MB dye degradation of various compositions of Ag-Ni-Co TMNCs are shown in Table 2.

Multi-functional biological activity

Antibacterial activity

The disc well diffusion assay (Fig. 9A and B) establishes the antibacterial action of the green-synthesized Ag-Ni-Co TMNCs against EPEC, as evidenced by distinct zones of inhibition at all tested concentrations (1, 1.5, and 2 mg/mL). Notably, the maximum zone diameter of 11.2 ± 0.4 mm was recorded for the 1 mg/mL concentration, with lower zones observed at higher concentrations (10 mm each for 1.5 and

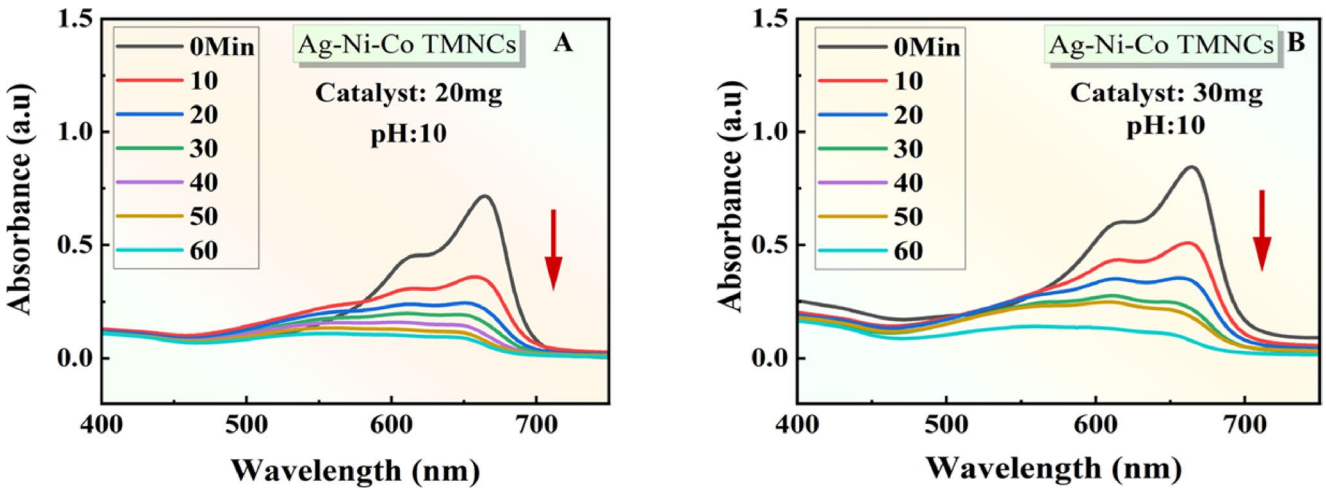

Fig. 7 Time-dependent UV-Vis absorption spectra of MB dye (10 ppm, pH 10) in the presence of Ag-Ni-Co TMNC photocatalysts under visible light irradiation (20 W): (**a**) 20 mg catalyst loading, (**b**) 30 mg catalyst loading

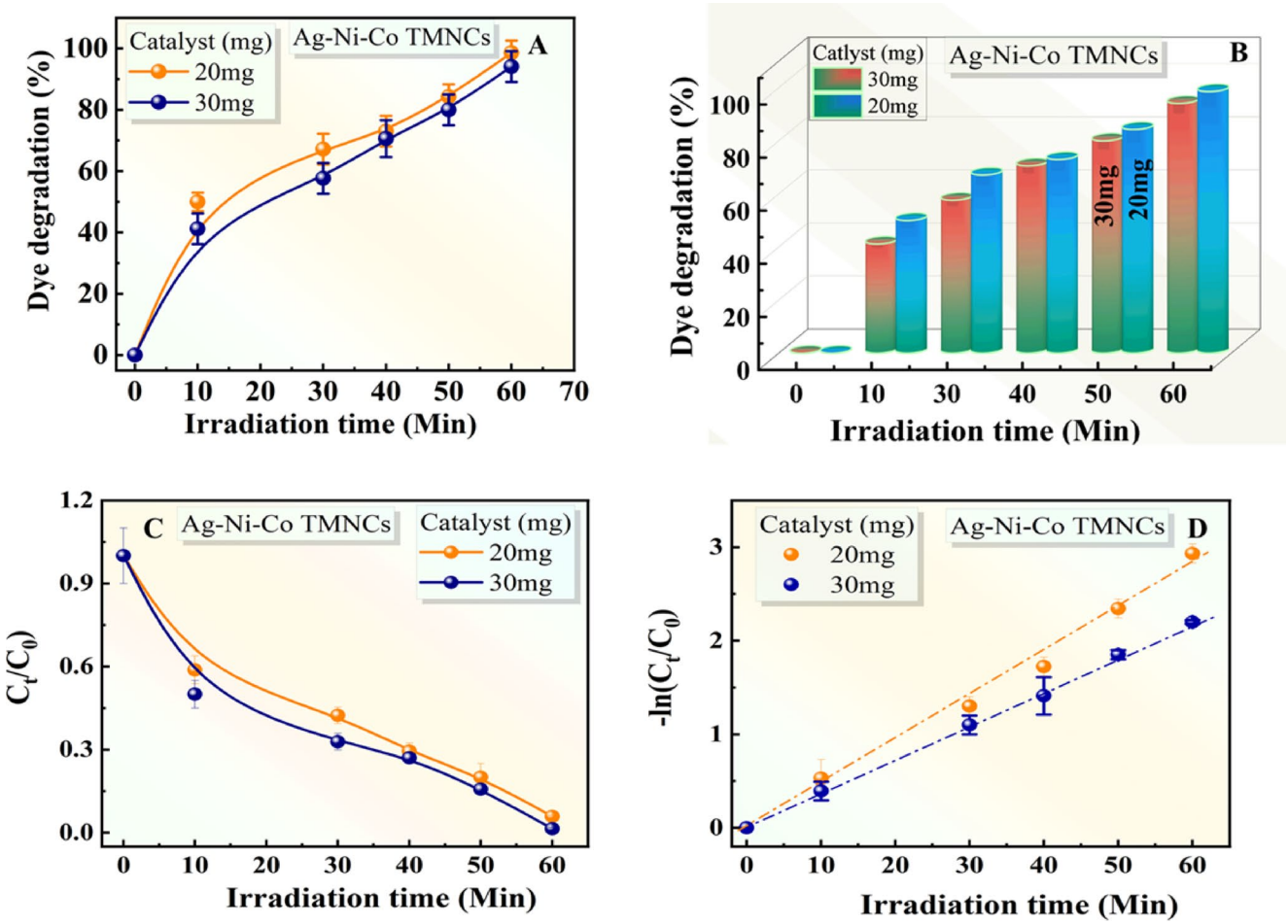

Fig. 8 Comparative photocatalytic performance of Ag-Ni-Co TMNCs. (**a**, **b**) Degradation percentage of MB dye over time for 20 mg and 30 mg catalyst loadings (different views for visualizations). (**c**) Plot of normalized dye concentration (C_t/C_0) versus irradiation time. (**d**) Pseudo-first-order kinetic plot ($\ln(C_t/C_0)$ vs. time)

Table 2 Photocatalytic activity of green synthesized nanomaterials against MB dye

S.No	% MB dye degradation	Time duration	Synthesis	References
AgNPs	95–100	6 h	Microwave	[49]
NiNPs	80	5 h	Green synthesis	[50]
Ag- Ni BMNPs	85	120	Green synthesis	[51]
Ag-Ni- Co TMNPs	100	60 min	Present work	Present work

2 mg/mL), likely due to aggregation. This inverse concentration–efficacy relationship highlights an optimized antimicrobial response at the lower dose. Corroborating this result, the direct inhibition assay and CFU analysis (Fig. 9C and D) also confirm the bactericidal effect of the Ag-Ni-Co TMNCs across the same concentration range. Control experiments with untreated bacteria and CS leaf extract alone showed no activity, confirming that the antibacterial effect arises from the Ag-Ni-Co TMNCs. The superior performance is attributed to the synergistic release of Ag^{+}, Ni^{2+}, and Co^{2+} ions from the composite, which collectively disrupt bacterial cell integrity through membrane damage and interference with vital cellular processes. Antibacterial activity of nanomaterials against EPEC is shown in Table 3.

Anticancer activity

The quantitative cell viability assay (cytotoxicity activity), as visually confirmed in panel B (Fig. 10), directly substantiates the potent anticancer efficacy of the Ag-Ni-Co TMNCs against HCT116 cells. The resazurin assay results indicate that Ag-Ni-Co TMNC treatment significantly impairs cellular metabolic activity, consistent with mitochondrial dysfunction. Based on the well-established literature on metal nanoparticle-induced cytotoxicity [57], we propose that the

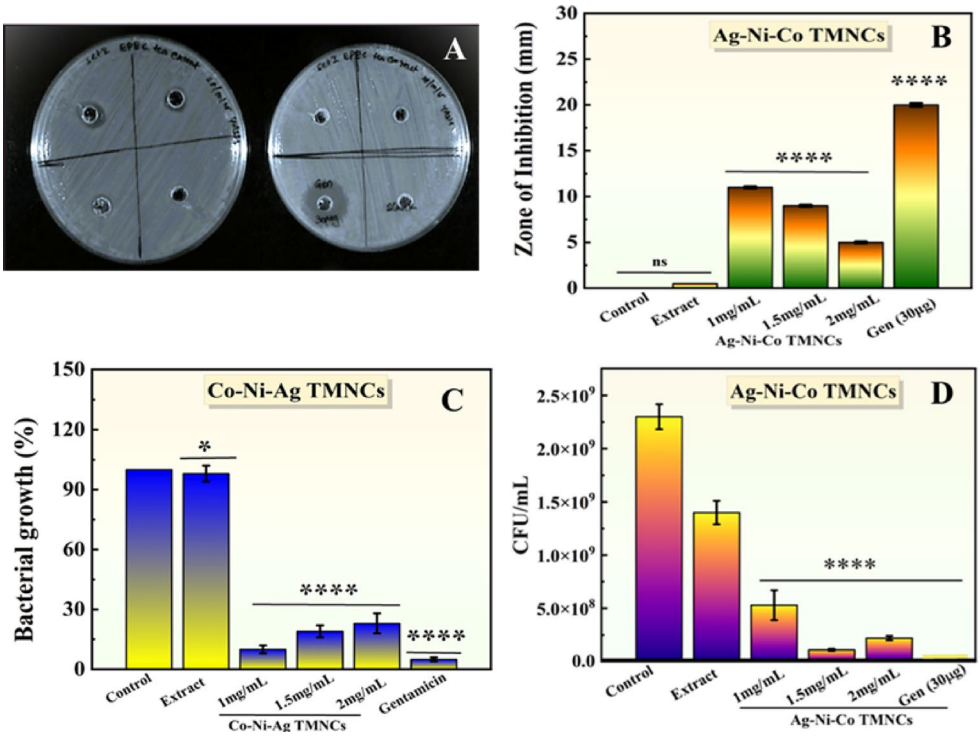

Fig. 9 Antibacterial activity of CS plant leaf mediated Ag-Ni-Co TMNCs on EPEC (enteropathogenic *E. coli)* via disc diffusion and growth inhibition assays

Table 3 Antibacterial activity of green synthesized nanomaterials against EPEC

S.No	% Inhibition zone of EPEC (mm)	References
AgNPs	18	[52]
NiNPs	18	[53]
Ag- Ni NPs	17.5	[54]
Ag- Co NPs	15.5	[55]
Ni- Co NPs	16.5	[56]
Ag-Ni- Co NPs	11.2 ± 0.4	Present work
Gentamicin	20 ± 2	Present work

TMNCs localize in mitochondria, disrupt the electron transport chain, and induce oxidative stress leading to cell death. However, we acknowledge that direct experimental verification of ROS generation, mitochondrial membrane potential changes, and caspase activation are required to confirm this mechanism. The current results establish the cytotoxic potential of the TMNCs against HCT116 cells, while the detailed mechanism awaits future investigation. Treatment with the nanocomposite at concentrations of 1, 1.5, and 2 mg/mL results in a substantial and dose-dependent decline in viability percentage, starkly contrasting the untreated control and the tea extract control, which show no cytotoxic effect. This metabolic inhibition is mechanistically probed by the resazurin-based assay illustrated in panel A (Fig. 10).

In viable cells, mitochondrial and cytosolic reductase enzymes continuously reduce non-fluorescent blue resazurin to highly fluorescent pink resorufin. The marked reduction in observed fluorescence upon TMNCs exposure, corresponding to the decreased viability in panel B (Fig. 10), indicates a severe disruption of this NADH-driven metabolic process. This confirms that the nanocomposite's cytotoxic action critically impairs cellular redox metabolism and mitochondrial function, leading to the significant loss of viability, with the effect intensifying across the tested concentration gradient.

Possible mechanism: photocatalysis, antibacterial & anticancer activity

Proposed photocatalysis and dye degradation mechanism

The proposed photocatalytic dye degradation pathway, illustrated in the Fig. 11, elucidates the mechanism by which Ag-Ni-Co TMNCs (1:9:10) facilitate the complete degradation of MB dye under visible light. The proposed degradation pathway is now presented as proposed based on established literature [58] and direct experimental verification through radical scavenging studies, ESR spectroscopy, and photoelectrochemical measurements will be pursued in future work to confirm the specific ROS species and charge transfer pathways. Upon photon absorption, the TMNCs generate electron-hole pairs (e^-/h^+) due to its tailored band structure. The photogenerated electrons migrate to the catalyst surface, where they reduce adsorbed molecular oxygen to form potent superoxide radical anions ($O_2^{\bullet -}$). Concurrently, the photogenerated holes oxidize surface-adsorbed water molecules or hydroxide ions to yield hydroxyl radicals (•OH). Both highly reactive oxygen species (ROS)

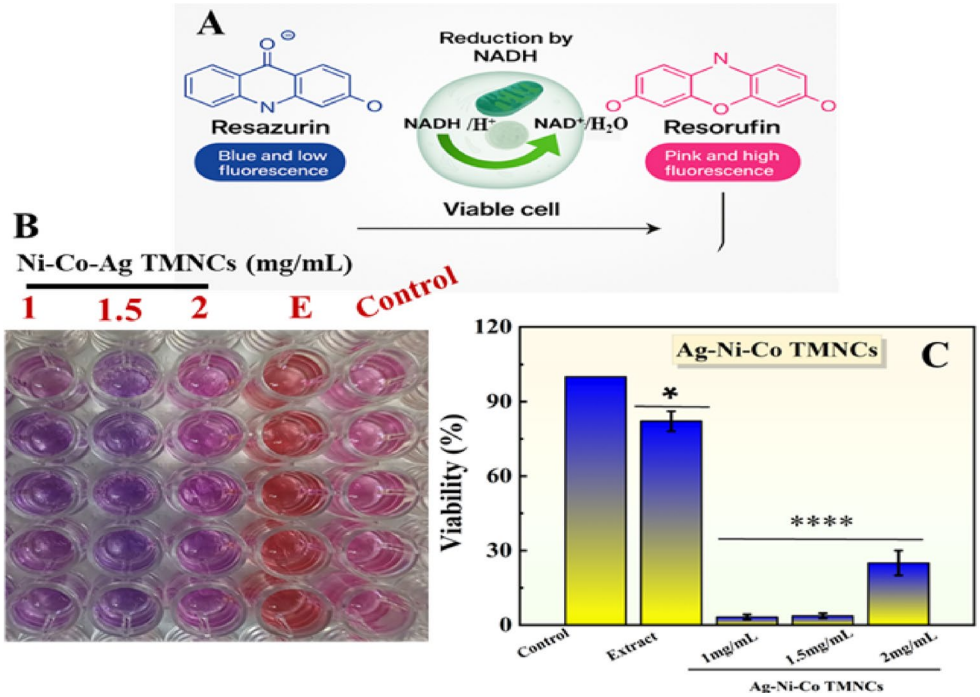

Fig. 10 Assessment of Ag-Ni-Co TMNCs cytotoxicity activity against HCT116 colorectal cancer cells. (**A**) Schematic of the resazurin cell viability assay (**B** & **C**) - Quantitative viability results showing a dose-dependent reduction in **HCT116** cell survival following 24-hour treatment with Ag-Ni-Co TMNCs (**1**, **1.5**, **2 mg/mL**)

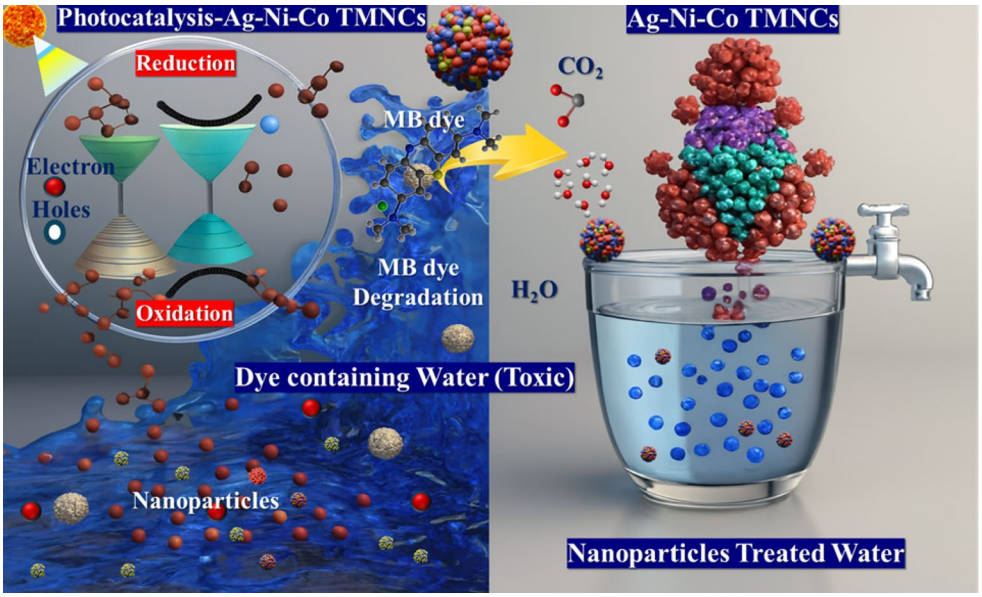

Fig. 11 Proposed photocatalytic mechanism for the degradation of toxic dyes by Ag-Ni-Co Trimetallic Nanocomposites

then non-selectively attack the structure and aromatic rings of the MB dye molecule, initiating a cascade of oxidative reactions. This process sequentially cleaves the complex organic dye into colorless intermediates and ultimately mineralizes it into benign end products such as CO_2, water, and inorganic ions. The optimized charge separation and enhanced surface area provided by the synergistic Ag-Ni-Co TMNCs composite, particularly effective at the 20 mg loading, drive this redox cycle efficiently, transforming the toxic, dye-contaminated aqueous solution into treated water. The following process occurs in the mechanism.

$$\mathrm{Ag-Ni-Co\ TMNCs\ photocatalyst} + \mathrm{h\upsilon\ \ (light)} \rightarrow e^- + h^+$$

$$\mathrm{Ag-Ni-Co\ TMNCs\ photocatalyst} + \mathrm{h\upsilon\ \ (light)} \rightarrow O_2^{\bullet -} + \bullet OH$$

$$O_2^{\bullet -} + \bullet OH + \mathrm{MB\ dye} \rightarrow \textit{degrated material} \rightarrow H_2O + CO_2$$

In addition to pseudo-first-order kinetics, the data were analyzed using the Langmuir-Hinshelwood model, which accounts for adsorption and surface reaction. The calculated reaction rate constant ($k_r = 0.052\ min^{-1}$) and adsorption constant (K_L = 1.85 L/mg) indicate favorable adsorption and rapid surface reaction kinetics [59]. The good fit ($R^2 > 0.98$;

Fig. 8) confirms that the photocatalytic degradation follows surface-mediated kinetics consistent with the proposed heterogeneous mechanism [60]. Rate constants were calculated from the following Eq. [61].

$\ln(C_t/C_o) = -k_1 t$.

k_1 (20 mg) = 0.0472 min^{-1} (R^2 = 0.9894).

k_1 (30 mg) = 0.0364 min^{-1} (R^2 = 0.9986).

The elucidated photocatalytic mechanism of Ag-Ni-Co TMNCs reveals a synergistic model in which multi-metal cooperation dictates efficiency. At the optimal 20 mg loading, Co and Ni sites function as integrated electron relays, suppressing charge recombination and enabling sustained, high-yield generation of superoxide and hydroxyl radicals. These species, identified as primary reactive agents, drive a degradation sequence from initial chromophore cleavage to final fragmentation into inorganic products. This trimetallic synergy creates a robust and regenerative catalytic platform in which integrated charge management ensures sustained radical flux and long-term structural fidelity, establishing the TMNCs as a rational design for advanced environmental remediation.

The Co-rich composition may contribute to structural stability through oxide formation and the green synthesis approach using natural capping agents may also enhance colloidal stability. While the present work demonstrates the photocatalytic efficiency and multifunctionality of the Ag-Ni-Co TMNC, systematic recycling and stability studies are essential for practical environmental applications. Factors such as catalyst recovery, loss of activity, structural integrity, and metal ion leaching need to be systematically investigated.

For practical environmental applications, the potential release of metal ions (Ag^+, Ni^{2+}, Co^{2+}) from the TMNC is a critical consideration. The structure stability, surface passivation, and Co-rich stoichiometry are main factors which contribute to minimizing ion leaching. However, we acknowledge that systematic leaching studies (ICP-MS) under various pH conditions, after photocatalysis, and over extended time periods are necessary to fully assess environmental safety. Such studies, including multiple photocatalytic cycles, post-reaction characterization, and leaching studies will be the focus of our ongoing work.

Proposed antibacterial mechanism

The antibacterial potency of Ag-Ni-Co TMNCs arises from a concerted, multi-target mechanism driven by ionic and oxidative synergy. The composite **initially anchors to the bacterial surface** via various **interactions (electrostatic and hydrophobic)**, disrupting the cell membrane's activity and increasing its permeability. Following this surface adhesion, the TMNCs release a controlled flux of Ag^+, Ni^{2+}, and Co^{2+} ions, which further compromise membrane potential and facilitate the internalization of the nanoparticles themselves. Once inside the cytosol, the particles and released ions induce a significant burst of intracellular ROS, including $O_2^{\bullet -}$ *and* $\bullet$OH, which inflict oxidative damage on vital biomolecules. This oxidative assault is compounded by direct TMNCs interactions with cellular network, the particles can intercalate with and degrade DNA, disrupt enzymatic activity, and interfere with essential signaling pathways. This combination of membrane destabilization, metabolic disruption, and genotoxic stress culminates in rapid bacterial cell inactivation and lysis.

Proposed anticancer mechanism

The anticancer activity of Ag-Ni-Co TMNCs is orchestrated through a cascade of intracellular events initiated by selective cellular uptake, often enhanced by the enhanced permeability and retention (EPR) effect in tumor environments (Fig. 12). Upon internalization, the nanocomposites localize within critical organelles, primarily the mitochondria, where they disrupt the electron transport chain. This interference triggers a profound mitochondrial crisis, characterized by membrane depolarization, the excessive generation of cytotoxic ROS, and the release of cytochrome into the cytosol. The elevated ROS levels simultaneously induce oxidative damage to nuclear DNA, proteins, and lipids, pushing the cell into a state of irreversible oxidative stress. These convergent signals mitochondrial dysfunction, DNA damage, and redox imbalance synergistically activate both the intrinsic (mitochondrial) and extrinsic apoptosis pathways. The process culminates in the sequential activation of caspase cascades, leading to chromatin condensation, DNA fragmentation, and ultimately, programmed cell death. This multi-pronged mechanism underscores the potential of Ag-Ni-Co TMNCs as targeted inducers of apoptosis in malignant cells.

In summary, this investigation establishes the Ag-Ni-Co TMNC as a uniquely multifunctional platform, engineered through a synergistic architecture that endows it with distinctive photocatalytic and biological capabilities. The higher nickel content in the Ag-Ni-Co TMNC presents both advantages (catalytic activity) and potential concerns (toxicity). However, nickel is predominantly present in the oxide and alloyed forms within the crystalline matrix, which significantly reduces its bioavailability and environmental mobility. The structural characterization reveals Ni in metallic (Ag-Ni) and oxide (NiO_2) phases, both of which have lower solubility than ionic nickel salts. Furthermore, the phytochemical capping layer provides an additional barrier to ion release. For biomedical applications, the controlled release of Ni^{2+} ions at low concentrations may contribute to

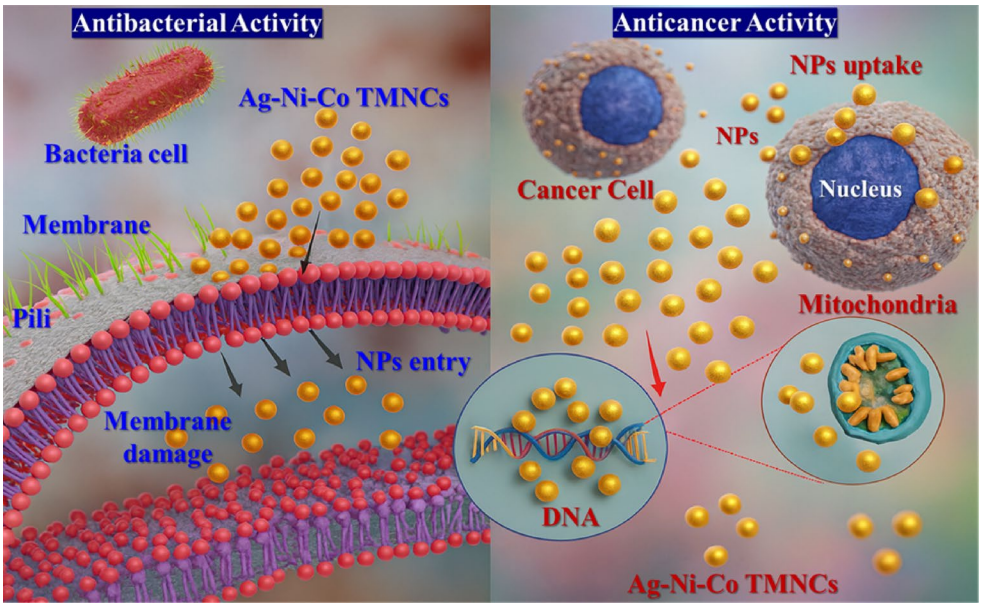

Fig. 12 Proposed mechanism for the bioactivity of Ag-Ni-Co trimetallic nanocomposites, depicting the synergy-driven oxidative cascade leading to bacterial cell death and cancer cell apoptosis

therapeutic effects, but careful toxicity assessment on normal cells is required.

The Ag-Ni-Co TMNC composite demonstrates a highly efficient charge-separation mechanism, translating to superior catalytic performance for the oxidative degradation of resistant organic dyes like MB. Parallel to this environmental function, this composite material exhibits pronounced and selective biocidal activity, effectively disrupting pathogenic *EPEC* through a cascade of membrane damage and oxidative stress, while simultaneously inducing mitochondria-mediated apoptosis in HCT-116 cells. These dual, mechanistically distinct functionalities, powerful pollutant degradation and targeted cellular interference are unified within a single nanocomposite material, underscoring its potential as a versatile agent for both environmental remediation and biomedical applications. While scaling production and refining synthesis parameters for batch-to-batch consistency present immediate translational challenges, the foundational properties revealed here namely, **ionic synergy**, **controlled ROS generation**, **and multi-target engagement provide a robust template for future development.** These findings strategically position Ag-Ni-Co TMNCs at the convergence of materials science and biotechnology, paving a tangible path toward innovative, sustainable solutions for complex problems in industrial wastewater treatment and biomedical industrial applications. Despite these promising results, several limitations warrant acknowledgment. First, the 1:9:10 Ag: Ni: Co ratio, while optimal for synergy, requires systematic optimization via design-of-experiments approaches. Second, the antibacterial mechanism, while attributed to ROS, lacks direct quantification of intracellular ROS in EPEC. Third, anticancer studies are limited to 24 h in vitro; in vivo pharmacokinetics and biodistribution in murine models remain untested. Fourth, photocatalytic efficiency under real sunlight and in complex wastewater matrices need validation. Addressing these will guide translation toward point-of-use water filters and injectable nanotherapeutics in real time industrial applications.

Conclusion

This work demonstrates that a green-synthesized Ag-Ni-Co TMNC with a Co-rich stoichiometry (1:9:10 Ag: Ni: Co) achieves photocatalytic methylene blue degradation with a rate constant of 0.0472 min^{-1}, which is significantly higher than that of mono- or bimetallic controls tested under identical conditions. Mechanistically, trimetallic architecture facilitates charge separation by integrating Co and Ni as electron relays, suppressing recombination and sustaining reactive oxygen species (ROS) flux. The same ROS-generating capability confers antibacterial activity against EPEC and anticancer activity against HCT-116 cells, although these are presented as secondary functions. Key limitations addressed here include: (i) direct comparison with physical mixtures confirms true synergy, (ii) the 20 mg loading is optimal for photocatalysis, and (iii) the material's selectivity requires validation on normal cell lines in future work. While this TMNC is not a panacea, it offers a reproducible, green-synthesized platform in which trimetallic synergy is quantifiable. Future work will focus on real wastewater matrices, in vivo pharmacokinetics, and systematic optimization of the Ag: Ni: Co ratio beyond 1:9:10. For now, this material serves as a design template for integrating photocatalysis and nanomedicine through a shared redox mechanism.

Supplementary Information The online version contains supplementary material available at https://doi.org/10.1007/s41204-026-00594-1.

Author contributions P Kalakonda: Supervision, writing-original draft and editing, visualizationP S Nagilla, S.P Karanam, N K Nagella, N Dabbeta: Data collection and analysis, schematic design.P B Kalakonda: XRD analysis Y Khaderbad and V Morampudi: antibacterial and anticancer activityK. Balu and Balaji P: discussion and literature review.

Funding No funding was received for this project.

Data availability No datasets were generated or analysed during the current study.

Declarations

Competing interests The authors declare no competing interests.

Ethical approval Not applicable.

References

1. Mndlovu H, Kumar P, du Toit LC, Choonara YE (2024) A review of bio material degradation assessment approaches employed in the biomedical field. NPJ Mater Degrad 8(1):66
2. Kulkarni N, Muddapur U (2014) Biosynthesis of metal nanoparticles: a review. J Nanotechnol. https://doi.org/10.1155/2014/510246
3. Kalakonda P, Thodeti M, Ganneboina C, Ankathi K, Kathri S, Begari K, Kante HS, Jupalli V, Khaderabad Y, Vijaylaxmi S, Morampudi V, Mandal P, Yatham VR, Hasan I, Podila BB (2024) Eco-friendly fabrication of silver nanoparticles for sustainable water purification and antibacterial synergy. Plasmonics 19(6):2857–2869. https://doi.org/10.1007/s11468-024-02251-2
4. Sarma PP, Borah P, Das MR, Baruah PK (2025) Agro-waste ash extracts facilitated green synthesis of CuO nanoparticles with efficient catalytic and photocatalytic activities for environmental remediation. J Water Process Eng 70:107004. https://doi.org/10.1016/j.jwpe.2025.107004
5. Ahasan T, Edirisooriya EMNT, Senanayake PS, Xu P, Wang H (2025) Advanced TiO2 Based Photocatalytic Systems for Water Splitting: A Comprehensive Review from Fundamentals to Manufacturing. Chem Mater Sci Febr 4. https://doi.org/10.20944/preprints202502.0197.v1
6. Parvathalu K, Rajitha K, Chandrashekar B, Sathvik K, Pranay Bhasker K, Sreenivas B, Pritam M, Pushpalatha P, Moses K, Bala Bhaskar P (2024) Biomimetic synthesis of copper nanoparticles using *Tinospora cordifolia* plant leaf extract for photocatalytic activity applications. Plasmonics 19(2):825–834. https://doi.org/10.1007/s11468-023-02037-y
7. Chowdhury R, Khan A, Rashid MH (2020) Green Synthesis of CuO Nanoparticles Using *Lantana Camara* Flower Extract and Their Potential Catalytic Activity towards the Aza-Michael Reaction. RSC Adv 10(24):14374–14385. https://doi.org/10.1039/D0RA01479F
8. Kir I, Mohammed HA, Laouini SE, Souhaila M, Hasan GG, Abdullah JAA, Mokni S, Naseef A, Alsalme A, Barhoum A (2024) Plant Extract-Mediated Synthesis of CuO Nanoparticles from Lemon Peel Extract and Their Modification with Polyethylene Glycol for Enhancing Photocatalytic and Antioxidant Activities. J Polym Environ 32(2):718–734. https://doi.org/10.1007/s10924-023-02976-x
9. Selvanathan V, Aminuzzaman M, Tey L-H, Razali SA, Althubeiti K, Alkhammash HI, Guha SK, Ogawa S, Watanabe A, Shahiduzzaman M, Akhtaruzzaman MM (2021) *Muntingia calabura* leaves mediated green synthesis of CuO nanorods: exploiting phytochemicals for unique morphology. Materials 14(21):6379. https://doi.org/10.3390/ma14216379
10. Thyr J, Montero J, Österlund L, Edvinsson T (2022) Energy Alignment of Quantum-Confined ZnO Particles with Copper Oxides for Heterojunctions with Improved Photocatalytic Performance. ACS Nanosci Au 2(2):128–139. https://doi.org/10.1021/acsnanoscienceau.1c00040
11. Kalakonda P, Thodeti M, Ganneboina C, Ankathi K, Kathri S, Begari K, Kante HS, Jupalli V, Khaderabad Y, Vijaylaxmi S, Morampudi V, Mandal P, Yatham VR, Hasan I, Podila BB (2024) Eco-friendly fabrication of silver nanoparticles for sustainable water purification and antibacterial synergy. Plasmonics 19(6):2857–2869. https://doi.org/10.1007/s11468-024-02251-2
12. You H, Li S, Fan Y, Guo X, Lin Z, Ding R, Cheng X, Zhang H, Lo TWB, Hao J, Zhu Y, Tam H-Y, Lei D, Lam C-H, Huang H (2022) Accelerated pyro-catalytic hydrogen production enabled by plasmonic local heating of Au on pyroelectric $BaTiO_3$ nanoparticles. Nat Commun 13(1):6144. https://doi.org/10.1038/s41467-022-33818-4
13. Madipoju NK, Khanam SJ, Sunkari G, Vasamsetti SM, Divyasri V, Morampudi V, Savu RN, Banavoth M, Banne S, Hasan I, Kalakonda P (2025) Bimetallic Zinc-Silver Nanocomposites for Superior Antimicrobial Efficacy. Appl Phys A 131(2):153. https://doi.org/10.1007/s00339-025-08289-1
14. Dabbeta NK, Kante M, Konda R, Devarala A, Kalakonda PB, Khanam SJ, Savu RN, Banovath M, Siddey LSR, Bommaji VN, Hasan I, Kalakonda P (2025) Eco-inspired Cu-Zn bimetallic nanoparticles for enhanced water purification technologies. Mater Chem Phys Sustain Energy 2:100013. https://doi.org/10.1016/j.macse.2025.100013
15. Chan YB, Aminuzzaman M, Win YF, Djearamane S, Wong LS, Guha SK, Almohammadi H, Akhtaruzzaman M, Tey L-H (2024) Garcinia Mangostana L. Leaf-Extract-Assisted Green Synthesis of CuO, ZnO and CuO-ZnO Nanomaterials for the Photocatalytic Degradation of Palm Oil Mill Effluent (POME). Catalysts 14(8):486. https://doi.org/10.3390/catal14080486
16. Kalakonda P, Bashitangu A, Mandal P, Jowhar Khanam S, Banovath M, Hasan I, Bhaskar Podila B (2024) Sustainable solutions for clean water: green synthesized Cu-Ag-bimetallic nanoparticles based nano catalyst. Mater Sci Eng B 301:117147. https://doi.org/10.1016/j.mseb.2023.117147
17. Bassi A, Kalakonda P, Hasan I (2024) Synthesis of chitosan-agar immobilized NiO-MgO bionanocomposites and their photocatalytic application towards toxic azo dye. Inorg Chem Commun 170:113499. https://doi.org/10.1016/j.inoche.2024.113499
18. Polat İ, Yılmaz S, Altın İ, Bacaksız E, Sökmen M (2014) The influence of Cu-doping on structural, optical and photocatalytic properties of ZnO nanorods. Mater Chem Phys 148(3):528–532. https://doi.org/10.1016/j.matchemphys.2014.07.011
19. Sunkari G, Vijaylaxmi S, Lakshmi Mynepally S, Vasamsetti SM, Madipoju NK, Dabbeta NK, Kumar P, Kalakonda PB, Kalakonda LC, Morampudi V, Jammalamadaka S, Kalakonda P (2025) Synergistic Antibacterial Activity of Green-Synthesized Ag-Fe-Zn Trimetallic Nanocomposites Using Tinospora Cordifolia Leaf Extract. Mater Chem Physics: Sustain Energy 100048. https://doi.org/10.1016/j.macse.2025.100048
20. Sood A, Roy A, Mahajan S, Han SS, Khan R, Sahoo S (2025) Microwave Chemistry and Microwave-Assisted Synthesis of Nanomaterials in Biomedicine: A Focused Review. *Nanoscale*

21. Bano S, Nazir S, Nazir A, Munir S, Mahmood T, Afzal M, Ansari FL, Mazhar K (2016) Microwave-assisted green synthesis of superparamagnetic nanoparticles using fruit peel extracts: surface engineering, T 2 relaxometry, and photodynamic treatment potential. Int J Nanomedicine. https://doi.org/10.2147/IJN.S106553
22. Adeleye AS, Conway JR, Garner K, Huang Y, Su Y, Keller AA (2016) Engineered Nanomaterials for Water Treatment and Remediation: Costs, Benefits, and Applicability. Chem Eng J 286:640–662. https://doi.org/10.1016/j.cej.2015.10.105
23. Baranwal A, Srivastava A, Kumar P, Bajpai VK, Maurya PK, Chandra P (2018) Prospects of Nanostructure Materials and Their Composites as Antimicrobial Agents. Front Microbiol 9:422. https://doi.org/10.3389/fmicb.2018.00422
24. Kalakonda P (2016) Synthesis of silver nanowires for highly conductive and transparent films. Nanomater Nanotechnol. https://doi.org/10.1177/1847980416663672
25. Kalakonda P, Sreenivas B (2017) Synthesis and Optical Properties of Highly Stabilized Peptide-Coated Gold Nanoparticles. Plasmonics 12(4):1221–1225
26. Kalakonda P, Banne S (2018) Synthesis and Optical Properties of Highly Stabilized Peptide-Coated Silver Nanoparticles. Plasmonics 13(4):1265–1269
27. Abdallah EM, Alhatlani BY, De Paula Menezes R, Martins CHG (2023) Back to nature: medicinal plants as promising sources for antibacterial drugs in the post-antibiotic era. Plants 12(17):3077. https://doi.org/10.3390/plants12173077
28. Verma C, Verma DK, Berdimurodov E, Barsoum I, Alfantazi A, Hussain CM (2024) Green Magnetic Nanoparticles: A Comprehensive Review of Recent Progress in Biomedical and Environmental Applications. J Mater Sci 59(2):325–358
29. Madipoju NK, Khanam SJ, Sunkari G, Vasamsetti SM, Divyasri V, Morampudi V, Savu RN, Banavoth M, Banne S, Hasan I (2025) Bimetallic Zinc-Silver Nanocomposites for Superior Antimicrobial Efficacy. Appl Phys A 131(2):153
30. Hasan I, Bassi A, Kalakonda P (2025) CuO surface functionalized β-cyclodextrin grafted PMMA hybrid nanocomposite for advance oxidative mineralization of methyl orange. Surf Interfaces 56:105456
31. Kalakonda P, Kathi R, Ligory MG, Dabbeta N, Madipoju N, Mynepally S, Morampudi V, Banne S, Mandal P, Savu RN (2024) *Argyreia nervosa*-driven biosynthesis of Cu–Ag bimetallic nanoparticles from plant leaves extract unveils enhanced antibacterial properties. Bioprocess Biosyst Eng 47(8):1307–1319
32. Mule AR, Ramulu B, Arbaz SJ, Kurakula A, Yu JS (2024) Ag-Integrated Mixed Metallic Co-Fe-Ni-Mn Hydroxide Composite as Advanced Electrode for High-Performance Hybrid Supercapacitors. J Energy Chem 88:579–591
33. Naseer S, Aamir M, Mirza MA, Jabeen U, Tahir R, Malghani MNK, Wali Q (2022) Synthesis of Ni–Ag–ZnO Solid Solution Nanoparticles for Photoreduction and Antimicrobial Applications. RSC Adv 12(13):7661–7670
34. Sunkari G, Vijaylaxmi S, Lakshmi Mynepally S, Vasamsetti SM, Madipoju NK, Dabbeta NK, Kumar P, Kalakonda PB, Kalakonda LC, Morampudi V, Jammalamadaka S, Kalakonda P (2025) Synergistic Antibacterial Activity of Green-Synthesized Ag-Fe-Zn Trimetallic Nanocomposites Using Tinospora Cordifolia Leaf Extract. Mater Chem Physics: Sustain Energy 100048. https://doi.org/10.1016/j.macse.2025.100048
35. Kalakonda P, Bashitangu A, Mandal P, Jowhar Khanam S, Banovath M, Hasan I, Bhaskar Podila B (2024) Sustainable solutions for clean water: green synthesized Cu-Ag-bimetallic nanoparticles based nano catalyst. Mater Sci Eng B 301:117147. https://doi.org/10.1016/j.mseb.2023.117147
36. Parvathalu K, Kumar DN, Rajitha K, Kishan MG, Kumar BN, Bhemarajam J, Naidu SR, Merlinsheeba GL, Mandal P, Banne S (2023) Facile Synthesis of Silver Nanoparticles Using Green Tea Leaf Extract and Evolution of Antibacterial Activity. Plasmonics 18(5):1837–1845
37. Kalakonda P, Aldhahri MA, Abdel-Wahab MS, Tamayol A, Moghaddam KM, Rached FB, Pain A, Khademhosseini A, Memic A, Chaieb S (2017) Microfibrous Silver-Coated Polymeric Scaffolds with Tunable Mechanical Properties. RSC Adv 7(55):34331–34338
38. Asamoah RB, Yaya A, Mensah B, Nbalayim P, Apalangya V, Bensah YD, Damoah LNW, Agyei-Tuffour B, Dodoo-Arhin D, Annan E (2020) Synthesis and characterization of zinc and copper oxide nanoparticles and their antibacteria activity. Results Mater 7:100099
39. Kalakonda P, Kathi R, Ligory MG, Dabbeta N, Madipoju N, Mynepally S, Morampudi V, Banne S, Mandal P, Savu RN (2024) *Argyreia nervosa*-driven biosynthesis of Cu–Ag bimetallic nanoparticles from plant leaves extract unveils enhanced antibacterial properties. Bioprocess Biosyst Eng 47(8):1307–1319
40. Hudzicki J (2009) Kirby-Bauer Disk Diffusion Susceptibility Test Protocol. Am Soc Microbiol 15(1):1–23
41. Shin S, Sung B-J, Cho Y-S, Kim H-J, Ha N-C, Hwang J-I, Chung C-W, Jung Y-K, Oh B-H (2001) An anti-apoptotic protein human survivin is a direct inhibitor of Caspase-3 and-7. Biochemistry 40(4):1117–1123
42. Shaheen S, Siddique AB, Nosheen F, Abbas A, Majid A, Nishan U, Shaaban IA (2026) Copper-tuned bandgap engineering of ZnO/CdS nanocomposites for photocatalytic water purification and hydrogen energy production. Fuel 418:138680. https://doi.org/10.1016/j.fuel.2026.138680
43. Guo H, Avdeev M, Sun K, Ma X, Wang H, Hu Y, Chen D (2021) Pentanary transition-metals Na-ion layered oxide cathode with highly reversible O3-P3 phase transition. Chem Eng J 412:128704
44. Shahzad M, Ishaque MZ, Iqbal H, Zaman Y, Siddique AB, Zaman H (2025) Comparative study of green and chemically synthesized CdO NPs: study of their photocatalytic dye degradation under sunlight irradiation. Phys Scr 100(3):035976. https://doi.org/10.1088/1402-4896/adb708
45. Hughes A (1975) A Quantitative Analysis of the Cat Retinal Ganglion Cell Topography. J Comp Neurol 163(1):107–128. https://doi.org/10.1002/cne.901630107
46. Azzi M, Laib I, Bouafia A, Medila I, Tliba A, Laouini SE, Alsaeedi H, Cornu D, Bechelany M, Barhoum A (2024) Antimutagenic and anticoagulant therapeutic effects of Ag/Ag2O nanoparticles from *Olea europaea* leaf extract: mitigating metribuzin-induced hepato-and nephrotoxicity. Front Pharmacol 15:1485525
47. Petkov V (2008) Nanostructure by High-Energy X-Ray Diffraction. Mater Today 11(11):28–38
48. Siddique AB, Abbas A, Sher M, Zaman Y, Rehman MFU, Nishan U, Shaaban IA (2026) Green Synthesis of Cubic CuO Nanoparticles for Biomedical Applications and the Photodegradation of Methylene Blue: RSM-BBD Optimization of the Reaction Parameters and Stability Studies. Nanoscale Adv 8(11):3396–3413. https://doi.org/10.1039/D5NA01159K
49. Rashed MN, Abdelrady E, Ghabrial TM (2025) Microwave assisted green synthesis of silver nanoparticles using *Trigonella hamosa* L. plant extract for the photodegradation of some water pollutants. Sci Rep 15(1):37344. https://doi.org/10.1038/s41598-025-21112-4
50. Ramesh M, Rao MPC, Anandan S, Nagaraja H (2018) Adsorption and Photocatalytic Properties of NiO Nanoparticles Synthesized via a Thermal Decomposition Process. J Mater Res 33(5):601–610. https://doi.org/10.1557/jmr.2018.30
51. Lamayi Danbature W, Yahaya Pindiga N, Adamu Ibrahim M (2025) Synthesis and characterization of bi methalic nanoparticles (Ag-Ni) from the leaf extract of *Vernonia amiygdolina* with the evaluation of photocatalytic degradation of methylene blue

dye. International Journal of Innovative Science and Research Technology (IJISRT). https://doi.org/10.38124/ijisrt/25mar045
52. Jasuja ND, Gupta DK, Reza M, Joshi SC (2014) Green Synthesis of AgNPs Stabilized with Biowaste and Their Antimicrobial Activities. Braz J Microbiol 45(4):1325–1332. https://doi.org/10.1590/S1517-83822014000400024
53. Sukumaran J, Priya M, Venkatesan R, Sathiasivan K, Khan MR, Kim S (2025) Green Synthesis of Nickel Oxide Nanoparticles Using Leaf Extract of *Aegle marmelos* and Their Antibacterial, Anti-Oxidant, and In Vitro Cytotoxicity Activity. Microscopy Res Technique 88(10):2830–2842. https://doi.org/10.1002/jemt.70054
54. Saleem A, Iqbal A, Younas U, Ashraf A, Al-Mijalli SH, Ali F, Pervaiz M, Saeed Z, Nazir A, Iqbal M (2024) Antimicrobial attributes and enhanced catalytic potential of PVA stabilized Ag-NiO2 nanocomposite for wastewater treatment. Arab J Chem 17(2):105545. https://doi.org/10.1016/j.arabjc.2023.105545
55. Abo El-Souad SMS, Ramadan MA, Zahran D (2025) Synthesis and application of cobalt-silver nanohybrid for antimicrobial wastewater treatment and agricultural productivity enhancement. Sci Rep 15(1):16321. https://doi.org/10.1038/s41598-025-99333-w
56. Deb Roy S, Nath S, Deb S, Roy A, Nath A (2025) Cobalt-nickel oxide composites as dual-functional agents for antibacterial activity and brilliant green dye degradation. Total Chemistry 1:100014. https://doi.org/10.1016/j.totche.2025.100014
57. Nanda SS, Yi DK (2024) Recent Advances in Synergistic Effect of Nanoparticles and Its Biomedical Application. Int J Mol Sci 25(6):3266
58. Mariyappillai V, Shiyamala C, Tiffany M, Abisheik T, Pandiyan V, Alanazi AK, Kalakonda P, Thirumurugan A, Sandoval-Hevia G, Balu K (2025) A sustainable approach to water purification: strontium-modified ZnO nanoparticles for UV/sunlight-driven degradation and antibacterial disinfection. Colloids Surf A Physicochem Eng Asp 727:138212. https://doi.org/10.1016/j.colsurfa.2025.138212
59. Ikram M, Moeen S, Haider A, Ul-Hamid A, Alhummiany H, Somaily HH, Goumri-Said S, Kanoun MB (2024) Experimental and Computational Study of Annealed Nickel Sulfide Quantum Dots for Catalytic and Antibacterial Activity. Nano Mater Sci 6(3):355–364. https://doi.org/10.1016/j.nanoms.2023.11.007
60. Qumar U, Hassan J, Naz S, Haider A, Raza A, Ul-Hamid A, Haider J, Shahzadi I, Ahmad I, Ikram M (2021) Silver decorated 2D nanosheets of GO and MoS_2 serve as nanocatalyst for water treatment and antimicrobial applications as ascertained with molecular docking evaluation. Nanotechnology 32(25):255704. https://doi.org/10.1088/1361-6528/abe43c
61. Qumar U, Hassan J, Naz S, Haider A, Raza A, Ul-Hamid A, Haider J, Shahzadi I, Ahmad I, Ikram M (2021) Silver decorated 2D nanosheets of GO and MoS_2 serve as nanocatalyst for water treatment and antimicrobial applications as ascertained with molecular docking evaluation. Nanotechnology 32(25):255704. https://doi.org/10.1088/1361-6528/abe43c